Extragalactic Astronomy and Cosmology Lab Report

Sofian Sakr, 3775830

2024, March

1 Exploring Friedmann Models in Cosmology

1.1 Introduction

The Friedmann equation relates the rate of expansion of the universe to the energy content of the universe. By integrating this equation, we can determine essential properties of the universe, such as creating Friedmann models for given sets of parameters and visualizing them. Determining the age of the universe, for these models. Comparison to analytic solutions, investigating collapse conditions, and studying energy density evolution.

Throughout this exercise, we leverage Python scripts to implement numerical computations and visualizations. These scripts enable us to explore various Friedmann models and investigate their implications based on different sets of cosmological parameters.

By combining theoretical insights with computational techniques, we aim to deepen our understanding of cosmological principles and phenomena.

1.2 Background

Here is the Friedmann-Lemaître-Robertson-Walker (FLRW) model, which describes the large-scale structure and evolution of the universe based on the principles of general relativity.

At the heart of the FLRW model lies the Friedmann equations, named after the Russian mathematician and physicist Alexander Friedmann, who derived them in the 1920s. These equations provide a set of differential equations that govern the expansion of the universe over time. They relate the rate of expansion, described by the scale factor $a(t)$, to the matter and energy content of the universe as:

$$\rho_{\mathrm{r}}(a) = \rho_{\mathrm{r}0} \left(\frac{1}{a^4} \right) \tag{1}$$

$$\rho_{\mathrm{m}}(a) = \rho_{\mathrm{m}0} \left(\frac{1}{a^3} \right) \tag{2}$$

$$\rho_{\Lambda}(a) = \rho_{\Lambda 0} \tag{3}$$

where $\rho_{\mathrm{r}0}$, $\rho_{\mathrm{m}0}$, and $\rho_{\Lambda 0}$ are the present-day radiation, matter, and dark energy density, respectively. In general, for a component with energy density ρ scaling as a^{-n}, the relation is given by:

$$\rho(a) = \rho_0 a^{-n} \tag{4}$$

where ρ_0 is the present-day energy density and n is the type of matter. For example, radiation has $n = 4$, matter has $n = 3$, and dark energy has $n = 0$.

The total energy density of the universe is given by the sum of the individual components:

$$\rho_{\mathrm{tot}}(a) = \rho_{\mathrm{r}}(a) + \rho_{\mathrm{m}}(a) + \rho_{\Lambda}(a) \tag{5}$$

The Friedmann equations take the following form:

$$H^2(a) = \left(\frac{\dot{a}}{a}\right)^2 = H_0^2 \left\{ \Omega_{\mathrm{r}} \frac{1}{a^4} + \Omega_{\mathrm{m}} \frac{1}{a^3} + \Omega_{\Lambda} + (1 - \Omega_{\mathrm{m}} - \Omega_{\Lambda} - \Omega_{\mathrm{r}}) \frac{1}{a^2} \right\} \tag{6}$$

With:

$$\frac{\mathrm{d}a}{\mathrm{d}t} = a\, H(a) \tag{7}$$

We integrate the right-hand side with respect to $a(t)$ to obtain t:

$$dt = \frac{1}{a \cdot \sqrt{H_0^2 \left\{ \Omega_{\mathrm{r}} \frac{1}{a^4} + \Omega_{\mathrm{m}} \frac{1}{a^3} + \Omega_{\Lambda} + (1 - \Omega_{\mathrm{m}} - \Omega_{\Lambda} - \Omega_{\mathrm{r}}) \frac{1}{a^2} \right\}}} \tag{8}$$

where $H(a)$ is the Hubble parameter, H_0 is the present-day Hubble constant, and Ω_{r}, Ω_{m}, and Ω_{Λ} are the radiation, matter, and dark energy density parameters, respectively. These equations describe the expansion rate of the universe as a function of time and its energy content.

1.3 Analysis

Using Python code, we calculated the age of the universe under two different sets of cosmological parameters, using the quad function to numerically integrate the integrand function. The results are printed out in Gyr (Gigayears) as the following:

Age of the universe (matter: 0.27, dark energy: 0.73, radiation: 0) is 14.328908319650155 Gyr
Age of the universe (matter: 0, dark energy: 1, radiation: 0) is 9.622982421889908 Gyr

Age of the universe (matter: 3, dark energy: 0.72, radiation: 0) is 14.005900563884824 Gyr

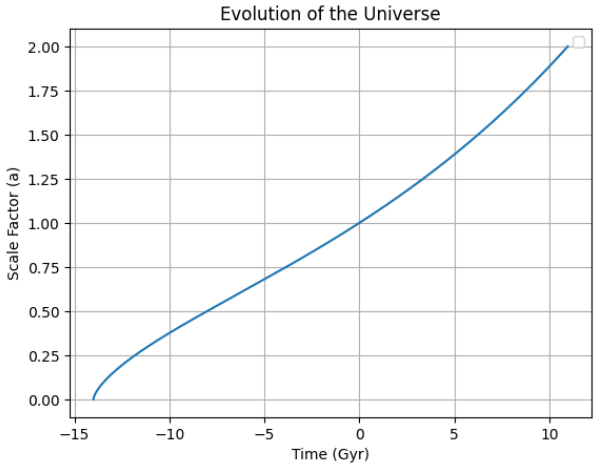

Figure 1.3.1: Scale factor over time plot

2 Malmquist bias

2.1 Introduction

The Malmquist bias is a significant concern in observational astronomy and cosmology, influencing our understanding of the universe's properties. This bias arises due to the inherent limitations and selection effects present in observational surveys, which can distort the observed properties of celestial objects. Understanding the Malmquist bias is crucial for accurately interpreting observational data and drawing reliable conclusions about cosmic phenomena.

In this section, we will explore the concept of the Malmquist bias in detail, discussing its origins, effects, and implications for astronomical research. We will also examine strategies for mitigating the Malmquist bias and improving the reliability of observational analyses. By gaining a deeper understanding of this bias, we can enhance the accuracy of our interpretations and advance our knowledge of the cosmos.

2.2 Exercise a: Plotting the Luminosity Distance

2.2.1 Background

Here, we explore the relationship between the comoving radial distance and the luminosity distance in cosmology. From the `astropy` package, we can obtain the time-dependent Hubble constant function, denoted as `cosmo.H(x)`, where x represents the redshifts as input.

We utilize the relations

$$v = H_0 D \tag{9}$$

and

$$v = zc \tag{10}$$

where H_0 denotes the Hubble constant, v represents velocity, D represents distance, z denotes redshift, and c denotes the speed of light.

Following Hubble's reasoning, since he used Cepheids to calculate the Hubble constant, we employ the relation

$$L = 4\pi D^2 \tag{11}$$

to determine the distance. I plot this distance against redshifts, extending the plot until $z = 1089$ (the redshift of the Cosmic Microwave Background).

Further analysis reveals that the flux received from a source is less than what is emitted due to two factors. Firstly, photons become redshifted as they travel to us due to the expansion of space. Secondly, the rate at which we receive the photons is less than the rate of emission, both of which reduce the flux. Considering these factors, we define the Luminosity distance.

2.2.2 Analysis

We obtain the luminosity distance using the function `cosmo.luminosity_distance(x)`. I plotted the luminosity distance against redshift on the same graph, observing that the luminosity distance is greater. This is consistent with the relationship

$$D_L = \frac{1}{a_e}\xi \tag{12}$$

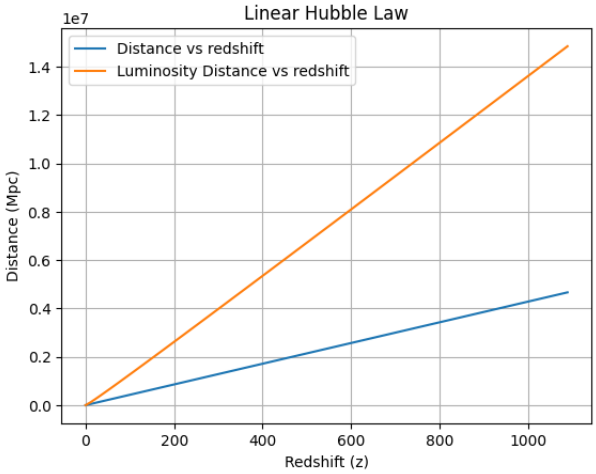

Figure 2.2.1: Luminosity distance plot

2.3 Exercise b: Detection Limit of Distant Sources

2.3.1 Analysis

In the context of the detection limit of distant sources, we conduct a scatter plot to visualize the distribution of galaxies. This distribution is characterized by two key properties: it is homogeneously random with respect to redshift and lognormal with respect to luminosity. Specifically, the luminosity distribution is centered around 10^{25} W.

To determine which galaxies will be observable in our survey, we establish a detection limit at $10^{-29}\,\mathrm{Wm}^{-2}$, representing the flux below which objects will not be observed. To ascertain the intrinsic luminosity required for detection at different redshifts, we leverage the relation $L = 4\pi D^2$, where L denotes luminosity and D represents distance. This relationship allows us to calculate the luminosity necessary for an object to be detectable at various redshifts.

By plotting the resulting curve derived from this intrinsic luminosity-redshift relationship, we can visually identify the threshold above which galaxies will be observable in our survey. Specifically, any object located above this curve will be detectable, while those below it will remain undetected.

This approach enables us to assess the detectability of galaxies across different redshifts and provides valuable insights into the limitations and capabilities of our observational survey. Additionally, it aids in determining the completeness of our dataset and helps ensure the accuracy of our findings regarding the distribution and properties of distant sources in the universe.

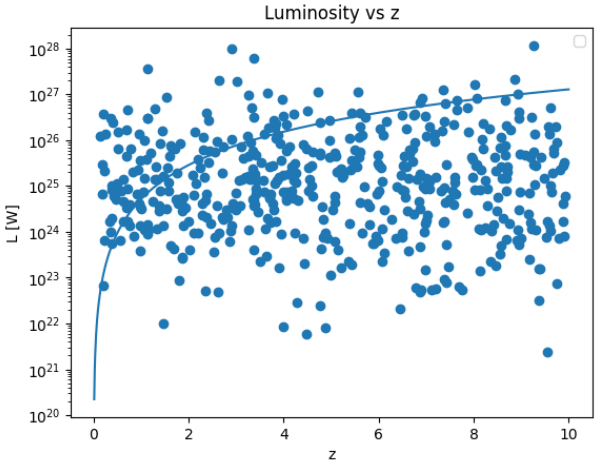

Figure 2.3.1: Detection limit and sources plot

2.4 Exercise c: Malmquist Bias with Two Properties

2.4.1 Analysis

Now, consider two properties, radio and X-ray, affected by telescope sensitivity. Only sources brighter in both radio and X-ray than the limiting flux density enter the sample.

Assume a random redshift distribution of the sources. Decide for each source if it is brighter than the limiting flux density in both radio and X-ray. Create a scatter plot of the two properties.

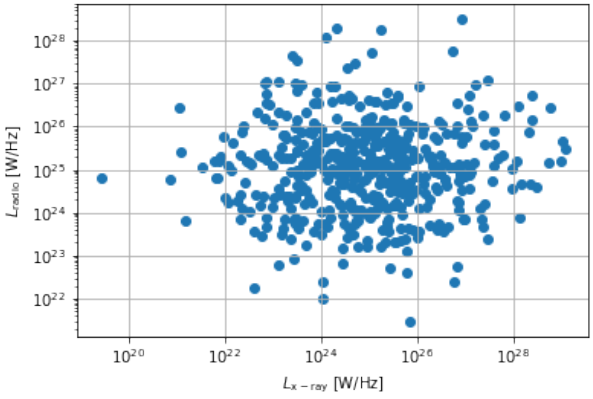

Figure 2.4.1: Sources that are brighter than the limiting flux density in both radio and X-ray scatter plot

2.5 Exercise d: Study the Correlation Coefficient

2.5.1 Analysis

Here, we calculate the minimum luminosity for radio and X-ray sources at a given redshift and flux limit, selects the sources that satisfy the condition, calculates the correlation coefficient between the logarithms of the X-ray and radio luminosities, and creates a scatter plot of the X-ray and radio luminosities.

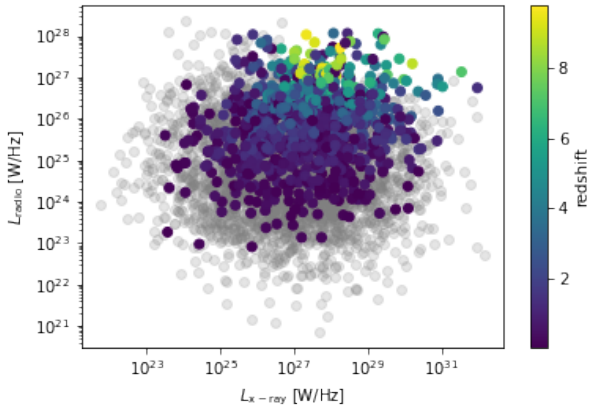

Figure 2.5.1: Sources detected and not detected in the observation with a sensitivity of 1 mJy in the X-ray and radio scatter plot

Correlation coeffecient 0.1591642791697024
No. of Sources detected in an observation with a sensitivity of 1 mJy: 881
No. of Sources not detected in an observation with a sensitivity of 1 mJy: 4119

2.6 Exercise e: Volume per Redshift Bin

2.6.1 Analysis

In real observations, the number of galaxies in each redshift bin is not equal. To model this dependence, divide the redshift range into bins, compute the volume for each bin, and choose a number of galaxies proportional to that volume. Join the redshift samples of all bins.

[0.34504192661370103, 0.6239347659976642, 1.1468233407597035]

3 Source Count

3.1 Introduction

Here, we are exploring a low-frequency astronomical survey, particularly the Low-Frequency Array (LOFAR) Two-metre Sky Survey (LoTSS). Getting the data via the Astron website. Our aim is to understand the flux density distribution of these astronomical sources in the dataset. For this purpose, we introduce the Differential Number Count, represented by: $\frac{dN}{dF}$ where N is the number of sources and F is the Flux. However, since N is a discrete variable, we cannot compute a continuous derivative. Therefore, we calculate the difference quotient $\frac{\Delta N}{\Delta F}$, ensuring that each flux bin contains at least 10 sources. Subsequently, we will plot graphs of $\frac{dN}{dF}$ against flux to visualize the distribution.

3.2 Background

Checking how the differential number count, N, varies with the flux densities of the flux bins in a Static Euclidean universe. Assuming all sources have identical luminosity, L, and are distributed isotropically, the flux F is given by $F = \frac{L}{4\pi D^2}$, which implies $F \propto \frac{1}{D^2}$. Thus, the distance D can be expressed as a function of F.

The number of sources is directly proportional to the volume V we are considering since the sources are isotropically distributed. The volume considered in each flux bin is $V = \frac{4}{3}\pi(D \cdot dF)^3$, so as we look at increasing flux bins, we are considering larger volumes, proportional to the cube of the distance. This implies $N \propto [D(F)]^3$, and with $D(F) = \left(\frac{L}{4\pi F}\right)^{-\frac{1}{2}}$, we get $N \propto \left(\frac{L}{4\pi F}\right)^{\frac{3}{2}}$. For the relationship between $\frac{dN}{dF}$ and flux, we take the derivative of this expression with respect to F, yielding $\frac{dN}{dF} \propto F^{-\frac{5}{2}}$.

3.3 Analysis

The search's central point and radius, as mentioned on the Astron website, must lie within the bounds of the surveyed area. To collect my data, I set the search for the position (195.54), and the number (5000)

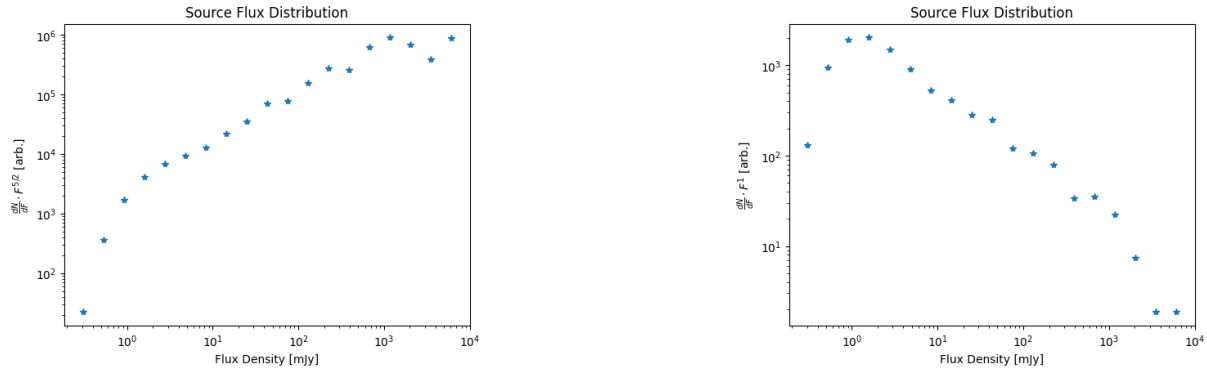

(a) with power of 5/2

(b) without power of 5/2

Figure 3.3.1: Sources count vs. flux density

4 Source Elevation

4.1 Introduction

The ability to observe a source using telescopes depends on whether it appears above the horizon. This is influenced by various factors including the nature of the source, the telescope's position, and the current time of year. I plan to chart the altitude of a specific source from the LOFAR dataset as observed from the Tautenburg Observatory today, in order to ascertain its visibility.

4.2 Analysis

I will be tracking the altitude of the source named ILTJ131132.92+440808.2 because it has a peak flux of 1.8 mJy/beam which is quite high. Retrieving the coordinates of the source in Python using the vo.dal.TAPService command. Plotting the altitude throughout the day 03.14.2024:

*Coordinates of source ILTJ*131132.92 + 440808.2 : 197.88716224101 44.135611075888

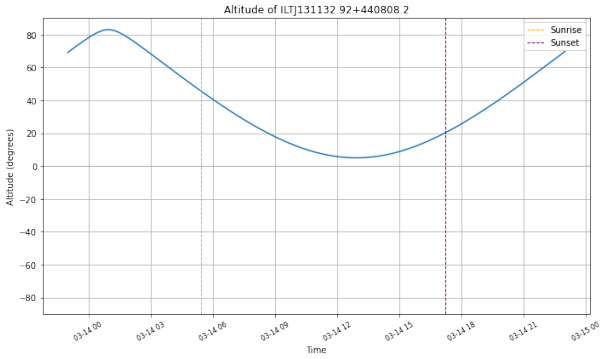

Figure 4.2.1: Altitude plot

5 SDSS Sky Server

5.1 Introduction

For this exercise, we'll use sky survey named SDSS. Unlike the LOFAR survey, SDSS spans a significantly broader area and operates within the visible range. We'll access the data from the dr16 interactive website. This platform also provides spectra for certain sources, enabling us to draw conclusions by examining emission lines, absorption lines, Lyman forest.

5.2 Analysis

I found a source that was both in SDSS and the LOFAR survey with a spectrum and analyzed it. In SDSS I found the source with the following spectrum:

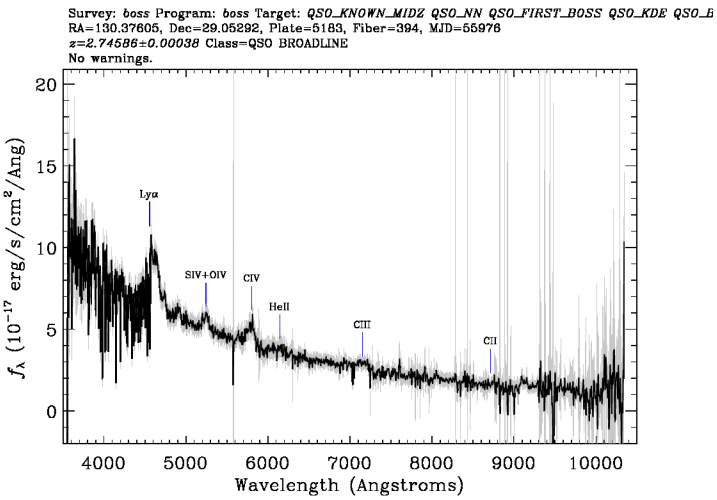

Figure 5.2.1: Broadline Spectrum

Upon checking the Astron Website, I discovered a source named ILTJ084046.90+290259.7 with coordinates RA = 130.195409909468 and Dec = 29.049936314506. I infer that this corresponds to the same object. If this object was observed in the LOFAR survey, it likely exhibits radio emission. In the spectrum, around 4000 Angstroms, we observe the Lyman Alpha forest, characteristic of quasars. Additionally, there is a broadening present, identified as Tag 4 in lecture slide 16. Based on these three observations, I conclude that this object is a broad-line quasar, consistent with the classification in SDSS.

6 FITS

6.1 Introduction

The Flexible Image Transport System (FITS) is a file format commonly used in astronomy to store and transmit scientific data, particularly images and tables. Developed in the late 1970s, FITS was designed to be flexible, efficient, and self-describing, making it ideal for handling astronomical data. It consists of two main parts: the header, containing metadata about the data, and the data itself, typically in the form of pixel values for images or tabular data for tables. FITS files are widely used in astrophysics research and are supported by many software tools and libraries in the field.

6.2 Analysis

To get the surface brightness profile we are going to be looking at how the brightness value of the pixels as you move out from the center. In DS9 we can create a shape and from Analyse we get the sum of the pixel brightness within the shape. We create an annulus(donut shape) centered at the center of the image at 250 against 250 pixels and we generate 100 annuluses moving out of the center.

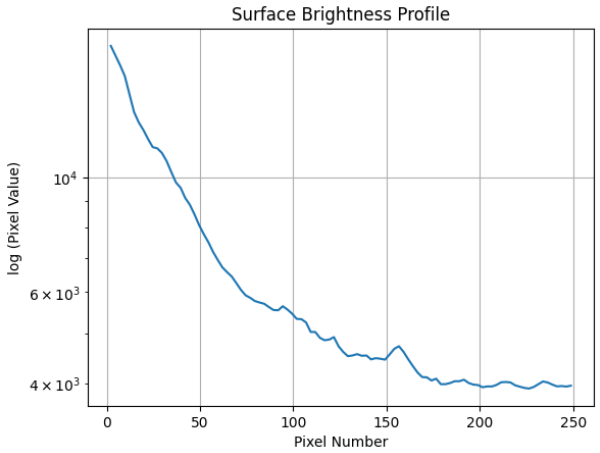

Figure 6.2.1: Surface Brightness Profile in the logarithmic scale

The X-axis represents the radius measured in pixels from the center, while the Y-axis displays pixel brightness on a logarithmic scale. Although the fits file provides a conversion factor from pixel brightness to flux unit, it's not required for this exercise. The graph exhibits exponential disk behavior, observable up to a specific threshold due to the log scale on the Y-axis. To identify the break in this exponential pattern, I employ linear regression.

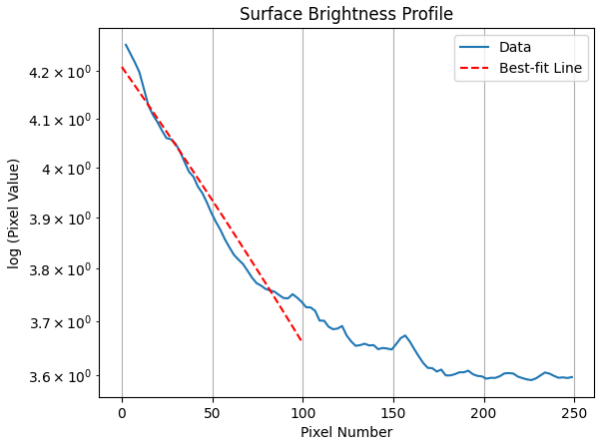

Figure 6.2.2: Best-fit-line for the surface brightness profile in the logarithmic scale

Beyond 100 pixels from the center, the signal diminishes into background noise, leading me to estimate the galaxy's radius. Given that each pixel in our image corresponds to 0.00047° in sky coordinates, my estimation suggests IC5332 spans a radius of 0.47 degrees. However, the publicly available data indicates the actual field radius to be 0.424 degrees. Despite this slight deviation, my calculation holds accuracy to two significant figures, supporting the conclusion that my surface brightness profile adequately models the exponential disk. To calculate the galaxy's radius in parsecs, we get the redshift (0.0023). Radius of the galaxy in parsecs: 8094.658615008867 pc

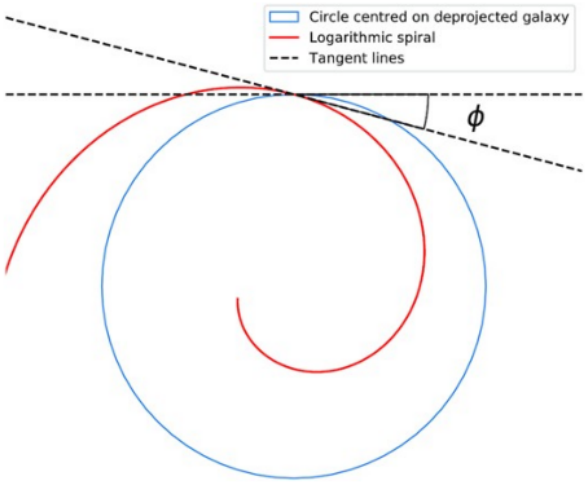

Figure 6.2.3: The pitch angle

The galaxy under observation is a spiral galaxy lacking a central bar. To classify, we estimate the pitch angle of its spiral arms. The pitch angle represents the angle formed between the tangent of a circle drawn around the galaxy's center and a tangent line to the logarithmic spiral of its arms. This involves identifying the straight line tangent to the circle and another tangent line to the spiral arm where it intersects the circle. Since the DS9 tool lacks the functionality to directly measure angles between lines, by constructing a triangle to facilitate angle calculation. Utilizing the compass tool ensured the triangle formed was right-angled. The pitch angle of 5 corresponds to a Sa Hubble-type galaxy.

$$\psi = \cos^{-1}\left(\frac{47.286462}{47.508813}\right) = 5.5455^\circ$$

7 Radio Contours

7.1 Introduction

Radio contours are graphical representations used in radio astronomy to visualize and analyze data from radio telescopes. These contours outline regions of similar radio intensity detected from celestial objects, such as galaxies, stars, and nebulae. The contours are typically overlaid on images or maps of the sky, providing a clear depiction of the distribution and structure of radio emission. Radio contours help astronomers identify features, such as sources of radio emission, and study their properties, such as size, shape, and brightness. We have sources that have a center and a diffused elliptical cloud around them are FR1 Active Radio Galaxies and if there are clear hotspots above and below they are FR2.

7.2 Analysis

I estimated the object to have a center around CRVAL: 161.084 59.6843, In the Astron website I belive this object is ILTJ104425.10+594139.8 because it has very hight Total Flux compared to others around this coordinate.

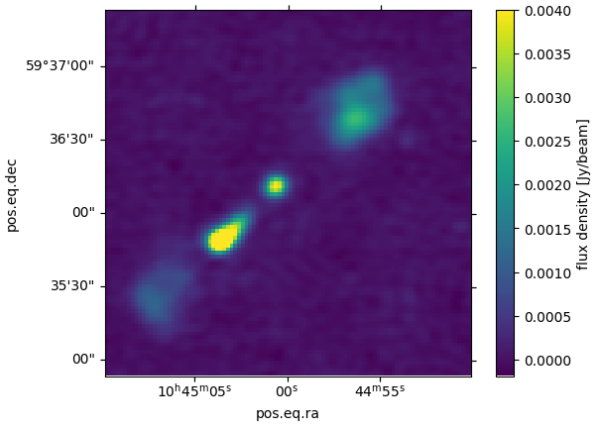

Figure 7.2.1: Enter Caption

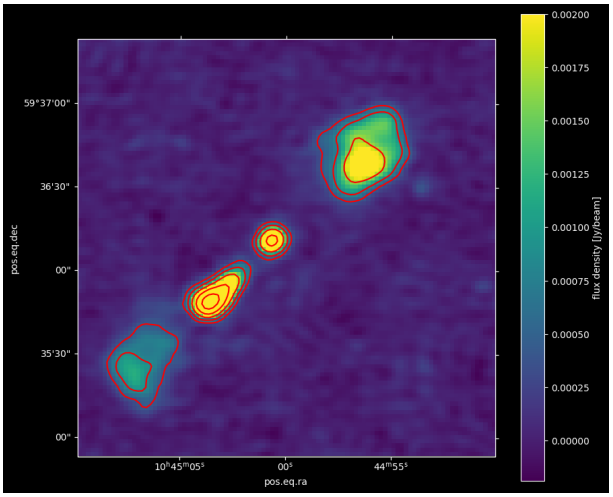

Figure 7.2.2: Enter Caption

8 RGB images and Contours

8.1 Analysis

Here we will overlay RGB images to check the final result.

- Object 1 Tailed Galaxy

This is a radio galaxy ILTJ171530.08+401138.2 in LOFAR(257.80833333, 39.69611111). Here the flux density color is logarithmic

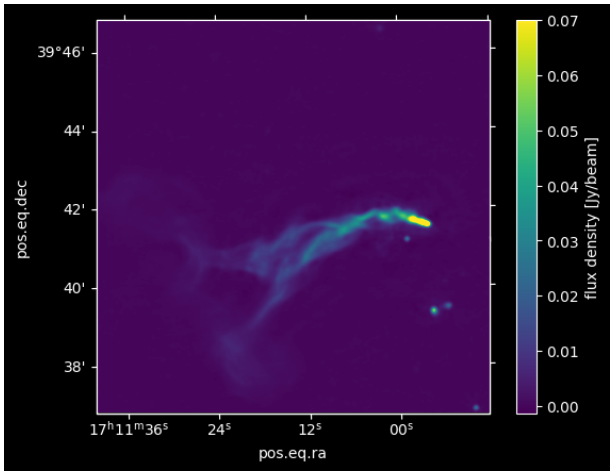

Figure 8.1.1: Tailed Galaxy

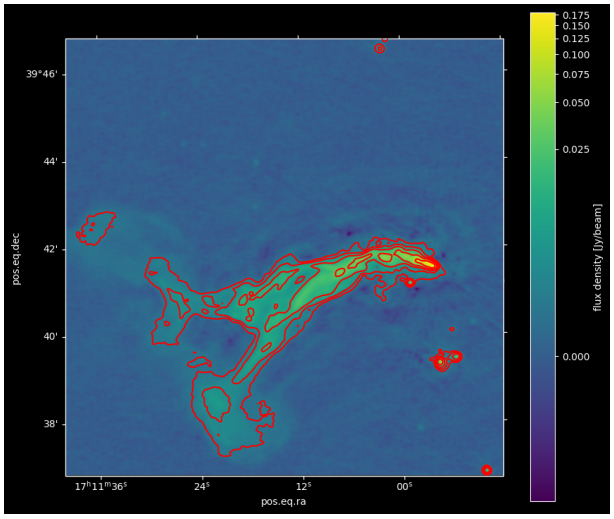

Figure 8.1.2: Contour lines over RGB image

There are at least two galaxies at the tip of the structure (area of brightest radio emission). My explanation on how this structure has been formed is that two radio galaxies were merging together and that's why we see two separate tails that combine into one. And, both of these galaxies are falling into a potential well.

9 Line Strength BPT: Luminosity vs Redshift Analysis

9.1 Introduction

For this exercise, I analyzed 9 sources, their spectra, fluxes, and both radio and optical images to classify these sources. Then, I plotted them on a Luminosity-Redshift graph to determine if the resulting curve matched the expected one, as discussed in Exercise 2.

9.2 Analysis

The following figures are the spectrum of 9 different objects with their respective redshifts and coordinates. I used the redshift value and the luminosity distance function to get the distance to the object. And then I used $L = 4\pi d^2 F$ to find Luminosity. But this luminosity is per Hz as we obtained the luminosity from flux density.

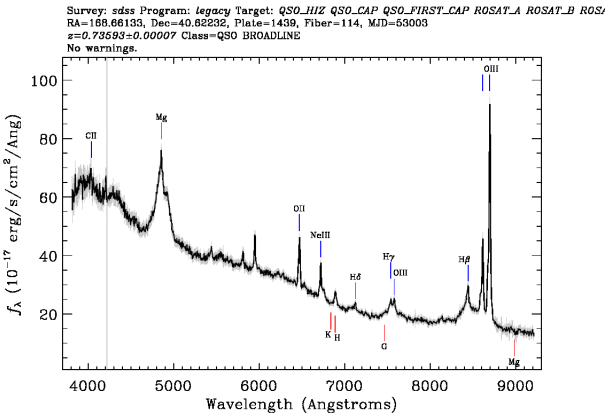

Figure 9.2.1: Object 1 Spectrum, Luminosity 1: 6.735771566450886 x $10^{28} WHz^{-1}$

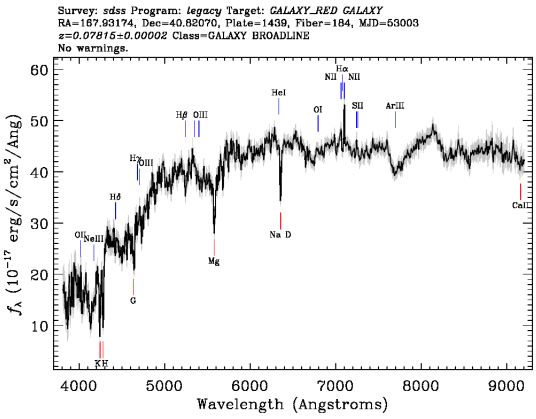

Figure 9.2.2: Object 2 Spectrum, Luminosity 2: 4.126164668478063 x $10^{26} WHz^{-1}$

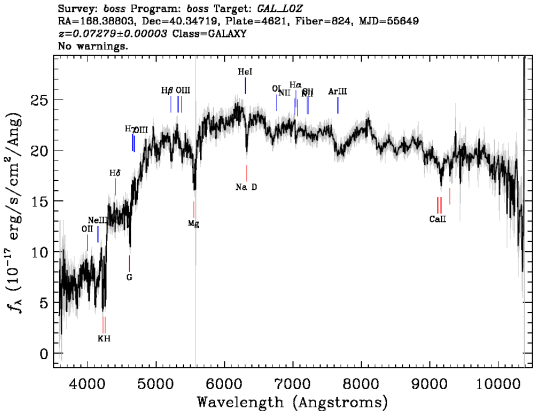

Figure 9.2.3: Object 3 Spectrum, Luminosity 3: 3.5530326498327594 x $10^{26} WHz^{-1}$

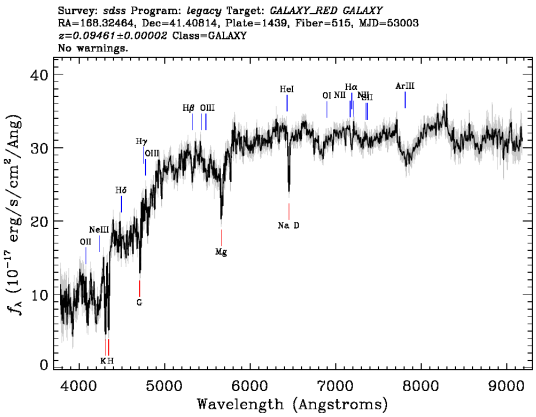

Figure 9.2.4: Object 4 Spectrum, Luminosity 4: 6.184966233409492 x $10^{26} WHz^{-1}$

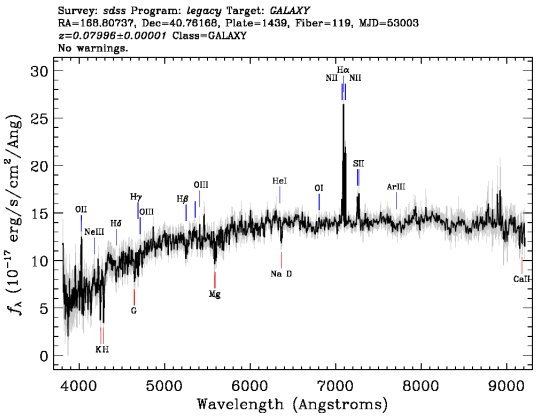

Figure 9.2.5: Object 5 Spectrum, Luminosity 5: 4.330322738596553 x $10^{26} WHz^{-1}$

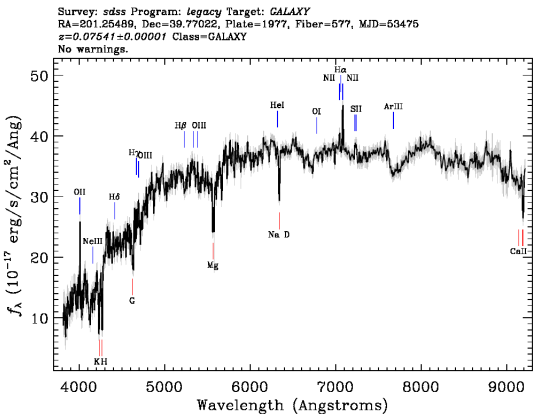

Figure 9.2.6: Object 6 Spectrum, Luminosity 6: 3.8273392955180026 x $10^{26} WHz^{-1}$

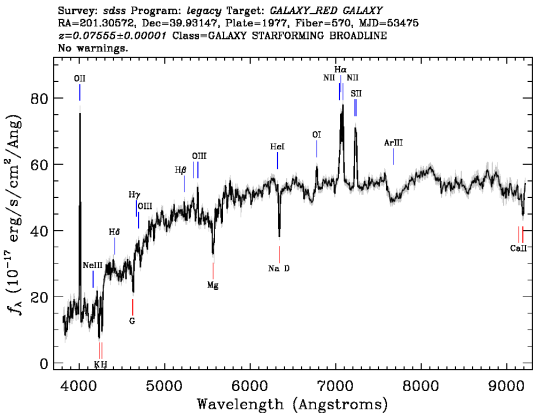

Figure 9.2.7: Object 7 Spectrum, Luminosity 7: 3.8423105059302776 x $10^{26} WHz^{-1}$

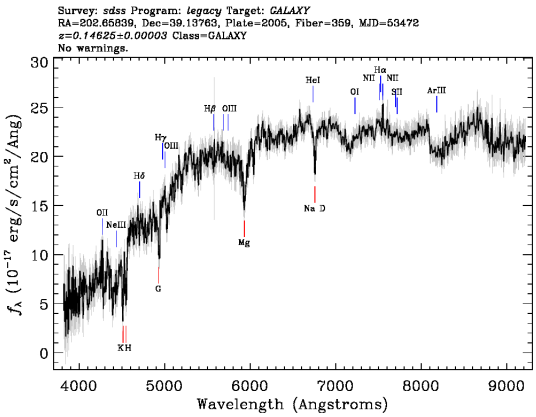

Figure 9.2.8: Object 8 Spectrum, Luminosity 8: 1.580844651929934 x $10^{27} WHz^{-1}$

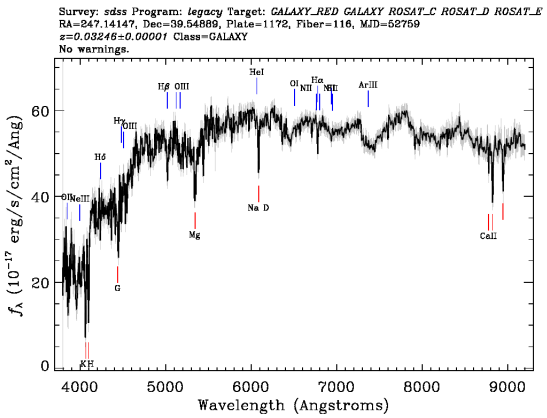

Figure 9.2.9: Object 9 Spectrum, Luminosity 9: 6.668243966059615 x $10^{25} WHz^{-1}$

After I calculated the luminosity calculation for all 9 objects, I plotted them on a graph against redshift with a logarithmic scale for luminosities:

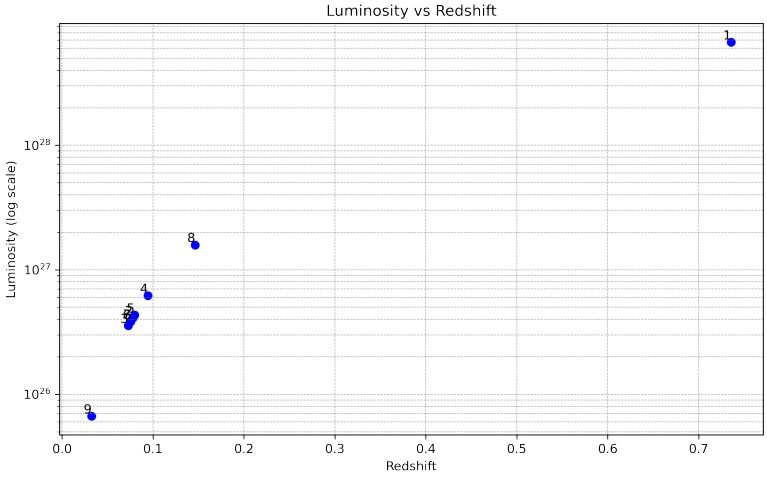

Figure 9.2.10: Luminosity vs Redshift plot

10 References

1. Friedmann equations: https://en.wikipedia.org/wiki/Friedmann_equations
2. Malmquist bias: https://en.wikipedia.org/wiki/Malmquist_bias
3. SDSS Data Release 18: https://cas.sdss.org/dr18/
4. SDSS SkyServer Search Form: https://skyserver.sdss.org/dr16/en/tools/search/form/searchform.aspx
5. Fanaroff-Riley classification: https://en.wikipedia.org/wiki/Fanaroff-Riley_classification
6. DS9 software: https://sites.google.com/cfa.harvard.edu/saoimageds9
7. Aladin Sky Atlas: https://aladin.cds.unistra.fr/
8. Lecture slides 22: https://moodle2.uni-leipzig.de/mod/resource/view.php?id=2405532
9. Lecture slides 17: https://moodle2.uni-leipzig.de/mod/resource/view.php?id=2394450